Attitude Reconstruction of Free-Flight CFD Generated Trajectories Using Non-Linear Pitch Damping Coefficient Curves

Quincy E. McKown*
NASA Ames Research Center, Moffett Field, CA 94035

Cole D. Kazemba† and Eric C. Stern‡
NASA Ames Research Center, Moffett Field, CA 94035

Joseph M. Brock§
Analytical Mechanics Associates, Inc., Moffett Field, CA 94035

Attitude history reconstruction of Free-flight CFD generated trajectories with non-linear pitch damping coefficient curves is investigated. Free-flight CFD simulations of the capsule shape used for the Genesis sample return mission and the upcoming Dragonfly mission to Titan are conducted for 1-, 2-, and 3-degree-of-freedom cases. Two different data reduction methodologies are employed to derive a pitch damping curve as a function of instantaneous angle of attack. These curves are then used to reconstruct the attitude history of the body which is compared to the raw simulation results. While both data reduction methods produce pitch damping curves that can generally reconstruct the motion seen in the Free-flight simulations, it is found that optimization of the pitch damping curve using an inverse estimation process yields superior and more generalizable results. Further refinement of this technique could allow pitch damping curves derived using CFD to serve as a capability complementary to existing techniques for dynamic stability characterization.

I. Nomenclature

A	=	analytical solution amplitude
C_A	=	axial force coefficient
C_D	=	drag force coefficient
C_{L_α}	=	lift slope with respect to α
C_{m_α}	=	pitch moment slope with respect to α
$(C_{m_q} + C_{m_{\dot{\alpha}}})$	=	pitch damping coefficient sum
d	=	diameter, m
I	=	moment of inertia, kg-m^2
k	=	spring damping coefficient
kg	=	kilogram
m	=	mass, kg
S	=	area, m^2
s	=	second
T	=	period of oscillation, s
t	=	time, s
V	=	velocity, m/s
x	=	horizontal distance downstream, m
α	=	angle of attack
γ	=	flight path angle
δ	=	analytical solution phase shift

*Aerospace Engineer, Pathways Student
†Aerospace Engineer, AIAA Member
‡Research Engineer, AIAA Member
§Aerothermodynamicist, AIAA Member

θ = pitch angle
ξ, μ = exponent of oscillation growth
ρ = density, kg/m^3
ω, ν = oscillation frequency, 1/s

subscript

0 = initial
∞ = free-stream
T = total

overscript

$\dot{y}$ = derivative
$\overline{y}$ = amplitude
$\hat{y}$ = estimate

II. Introduction

Trajectory reconstruction using non-linear pitch damping coefficient curves is investigated using unsteady Computational Fluid Dynamics (CFD) simulations and experimental ballistic range data. Free-flight CFD (FF-CFD) is a complementary capability to experimental techniques and provides a full time history of motion, forces, and moments. Conversely, ballistic range experimental data are limited to discrete observations of the vehicle orientation as determined by inspection of shadowgraph images taken at stations along the test range. The richer data-sets provided by FF-CFD provide an opportunity to expand the understanding of blunt body dynamic behavior. The dynamic oscillation growth or decay of an atmospheric flight vehicle is typically described with the pitch damping coefficient as a function of angle of attack and Mach number. This formulation is used in Monte Carlo studies using high-fidelity trajectory simulations to assess the probabilistic performance of entry vehicles as they traverse through a planetary atmosphere. It is crucial that these pitch damping curves accurately capture the complex dynamic behavior typical of blunt body vehicles. This work presents a method for implementing pitch damping curves derived from FF-CFD into trajectory simulations, proposes a new inverse estimation technique to determine the pitch damping curve, and assesses the performance of the resulting reconstructed trajectories relative to FF-CFD data.

Pitch damping curves are derived from FF-CFD data using two different methods. The first approach, detailed in Stern et al.[1], leverages the analytical expression from Schoenenberger and Queen [2] to find sectional fits of the pitch damping coefficient to a moving subset of the observed attitude peaks. After populating a set of local pitch damping coefficients from each subset of peaks across all of the FF-CFD data-sets, a non-linear curve is fit through the collection of sectional fits. The nonlinear function that is used for this curve fit is the Comprehensive Aerodynamic Data Reduction system for Aeroballistic Ranges (CADRA) [3] form that is described in Schoenenberger et al. [4]. Finally, the approach developed by Redd [5] is used to convert this pitch damping curve from its native amplitude-based formulation to an equivalent form as a function of instantaneous angle of attack that is suitable for application in trajectory simulations. Analysis of the relationship between the amplitude-based and instantaneous pitch damping curves is performed.

An alternative approach to determining the pitch damping curve as a function of instantaneous angle of attack is proposed. This scheme employs an inverse estimation methodology to solve for a pitch damping curve that is optimal for recreating the angle of attack behavior in the FF-CFD data. Implementation of this method involves sending a functional form of the pitch damping curve to an optimizer that wraps the aforementioned initial value reconstruction method. The objective function is the normalized L_2 difference between the reconstructed peak magnitudes and the actual peak magnitudes. The objective function can also be modified to include the normalized L_2 difference between the reconstructed peak times and the actual peak times, allowing for estimation of the pitch moment slope (which dictates the oscillation frequency) and the pitch damping simultaneously.

Evaluation of the pitch damping curves derived from each data reduction approach is conducted based on residuals of peaks in the total angle of attack, $\overline{\alpha_T}$ (i.e. amplitude of an oscillation cycle) when applied to a validation data-set.

III. Approach

The effort described in this work requires procedures for high-fidelity simulation of the free-flight behavior of a blunt body with varying degrees of translational and rotational freedom, determination of the pitch damping coefficient as a function of amplitude and instantaneous angle of attack, and propagation of the closed-form equations of motion using the derived pitch damping coefficient to predict capsule dynamics as a function of time or horizontal displacement.

Both methods explored in this work for estimating a pitch damping curve require knowledge of capsule attitude history. These trajectories are calculated here using the FF-CFD solver package available in US3D [6–8]. Studies to date using the FF-CFD capability have shown excellent agreement with experimental data across a range of geometries and Mach numbers [9–12]. The FF-CFD data includes initial conditions and the subsequent trajectory history; α_T, time, and velocity if the body is decelerating.

The first approach applied in this work uses analytical formulations for the pitch damping coefficient in 1-, 2-, and 3-degrees-of-freedom. The local pitch damping coefficient can be determined for a subsequent series of peaks, referred to as a stencil. This stencil is a subset of the full trajectory and the average $\overline{\alpha_T}$ of the peaks within a stencil is stored with the calculated pitch damping coefficient. The collection of these sectional fits is curve fit using a functional form expression of CADRA [4]. Next, this non-linear curve as a function of amplitude ($\overline{\alpha_T}$) is converted to a non-linear curve as a function of instantaneous angle of attack (α) using an approach presented by Redd [5]. The non-linear curve as a function of instantaneous angle of attack is used to reconstruct the attitude history with the initial conditions and static coefficients derived a priori. The reduced degree-of-freedom (DoF) solutions presented by Schoenenberger and Queen [2] (summarized below), are used to implement the reconstruction by integrating from the initial state forward in time. The actual and reconstructed attitude histories are then compared to determine the accuracy of the pitch damping curve.

The attitude history of a vehicle as a function of time can be simulated by solving a non-linear ordinary differential equation (ODE) initial value problem. This non-linear ODE in terms of angle of attack, α, is derived using blunt body planar equations of motion and can be solved in closed-form by applying simplifications based on reduced DoF cases [2]. With initial conditions, static coefficients, and a pitch damping curve, the ODE can be solved forward in time for α. This is accomplished using Runge-Kutta 45, a method of numerical integration of order $O(h^4)$ with an error estimator of order $O(h^5)$ [13].

Alternatively, the pitch damping curve can be found by using an inverse method that constructs a curve designed to minimize the residual between the reconstructed trajectory and the actual trajectory. This is done by sending an initial functional form of the pitch damping curve to the trajectory reconstruction scheme that integrates the equations of motion forward in time. The parameters defining the pitch damping curve are then iterated on in an optimization loop to minimize residuals between the reconstructed and actual trajectories and thereby identify an optimal curve. This procedure has been demonstrated with one degree-of-freedom (1-DoF) data and requires knowledge of the trajectory history (α_T time) and the parameters of the run, such as velocity, mass, and diameter.

A. Free-Flight CFD

We utilize the finite-volume flow solver US3D, which is an unstructured, Navier-Stokes solver that allows for mesh deformation to take the attitude changes of the capsule into account [6–8]. The program was run to simulate the conditions from the Genesis ballistic range test matrix as detailed by Cheatwood [14]. This involved geometric, mass, and velocity parameter matching. For reference, the mass of the model investigated was 0.633 kg and the diameter was 0.06942 m. A schematic showing key features of the ballistic range models is shown in Fig. 1. FF-CFD allows for reduced DoF simulations by eliminating selected rotational or translational degrees of freedom. This capability was leveraged to allow for direct application of the analytical solutions derived by Schoenenberger and Queen for determination of the pitch damping coefficient [2]. Processing of the FF-CFD data is implemented using a Python package to parse and store relevant information in a readable and accessible format.

For the upcoming Dragonfly mission, the intended Mach number for deployment of the drogue parachute is approximately 1.5 [15]. The Genesis ballistic range campaign only conducted one test at conditions near this critical point; shot R990407 had an initial Mach number of 1.88 and a final Mach number of 0.99, for an average Mach number of 1.44 [14]. To best simulate the experimental test conditions and to provide mission relevant insights at this critical regime, all simulations were run at a constant (1-DoF, two degrees-of-freedom (2-DoF)) or average (three degrees-of-freedom (3-DoF)) Mach number of 1.44.

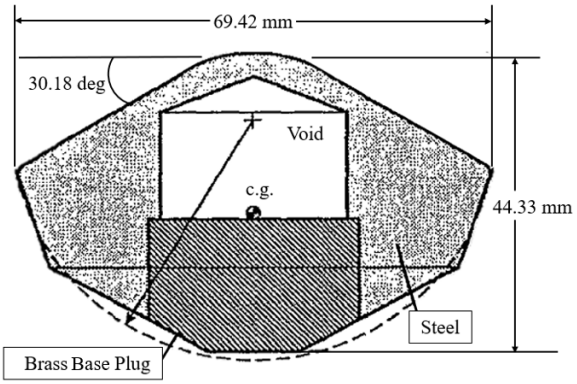

Fig. 1 Genesis ballistic range test model [14].

B. Aerodynamic Modeling with Analytical Solutions

With the readily constrained outputs of FF-CFD, the resulting dynamics can be described using the analytical formulations of the equations of motion presented by Schoenenberger and Queen [2]. These equations of motion assume the following:

- planar motion
- density (ρ) is constant
- small angles of attack (<30°)
- lift and pitching moment vary linearly with angle of attack
- the mean flight path angle (γ) over a trajectory segment is effectively constant with small sinusoidal variation due to lift for 2-DoF and 3-DoF trajectories (i.e. gravity and centrifugal effects are small).

Three cases with increasing degrees-of-freedom were considered. The solutions of this analysis will be presented, however detailed derivations are included in Reference [2]. Figure 2 illustrates the coordinate system used in this analysis. The pitch damping coefficient is extracted using a baseline planar ODE that captures oscillations and amplitude growth (see Eq. (1)). Each case makes simplifying assumptions to derive a solution from this baseline equation.

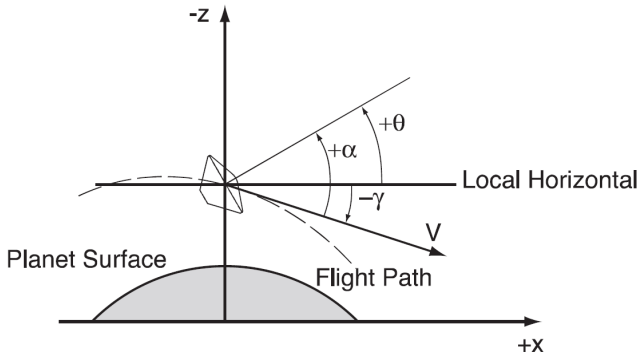

Fig. 2 Coordinate system.

$$\ddot{\alpha} - \frac{\rho V S}{2m}\left(-C_{L\alpha} + \frac{md^2}{2I}\left(C_{m_q} + C_{m_{\dot{\alpha}}}\right)\right)\dot{\alpha} - \frac{\rho V S d^2}{2I} C_{m_\alpha}\alpha = 0 \tag{1}$$

1. Free-to-pitch

The 1-DoF case models a single rotational DoF, referred to as "free-to-pitch". In Fig. 2, this is rotation about the y-axis and simulates a model constrained to rotate about a fixed axis through the vehicle center of mass in a wind tunnel

where velocity is constant. This eliminates any contribution from the lift force in the oscillation and thus $C_{L\alpha} = 0$ in Eq. (1). The equation can then be solved for α as a simple, harmonic oscillator as shown in Eq. (2), with the exponent of oscillation growth defined by Eq. (3) and the frequency of oscillation defined by Eq. (4).

$$\alpha = Ae^{\xi_1 t}\cos(\omega t + \delta) \tag{2}$$

$$\xi_1 = \frac{\rho V S d^2}{8I}(C_{m_q} + C_{m_{\dot{\alpha}}}) \tag{3}$$

$$\omega = \sqrt{-\frac{\rho V^2 S d}{2I} C_{m_\alpha}} \tag{4}$$

2. Free-to-pitch, free-to-heave

2-DoF is referred to as "free-to-pitch, free-to-heave" and allows the body to pitch as well as translate along the vertical axis, or the z-axis in Fig. 2. This set of conditions approximates a vertical wind tunnel test or a vehicle at terminal velocity where velocity is constant but the body can move transverse to the velocity vector due to lift. Similar to the 1-DoF case, solving Eq. (1) for 2-DoF also results in a simple harmonic oscillator formulation for α (Eq. (5)) with the same frequency as the 1-DoF case (Eq. (4)). However, because of the contributions from $C_{L\alpha}$, the exponential damping sum is different and given by Eq. (6), and since $C_{L\alpha}$ is negative for blunt bodies, its term in the exponent becomes a contributor to oscillation growth. In other words, the transverse motion due to lift can affect capsule oscillation growth.

$$\alpha = Ae^{\xi_2 t}\cos(\omega t + \delta) \tag{5}$$

$$\xi_2 = \frac{\rho V S}{4m}\left(-C_{L_\alpha} + \frac{md^2}{2I}(C_{m_q} + C_{m_{\dot{\alpha}}})\right) = \xi_1 - \frac{\rho V S}{4m} C_{L_\alpha} \tag{6}$$

3. Decelerating, free-to-pitch, free-to-heave

Finally, 3-DoF is referred to as "decelerating, free-to-pitch, free-to-heave" and includes the motion defined in 1-DoF and 2-DoF with the introduction of deceleration in response to the aerodynamic drag force. The velocity profile can be approximated using Eq. (7) assuming $C_D \simeq C_A$. Combining Eq. (1) and Eq. (7) results in the Euler-Cauchy equation, which is solved to give an analytical expression for α (Eq. (8)) with the exponent of oscillation growth given in Eq. (9) and the frequency given in Eq. (10) [16].

$$V = \frac{2m}{\rho S C_A t} \tag{7}$$

$$\alpha = At^{\mu}\cos(\nu \ln t + \delta) \tag{8}$$

$$\mu = \frac{1}{2} - \frac{C_{L_\alpha}}{C_A} + \frac{md^2\left(C_{m_q} + C_{m_{\dot{\alpha}}}\right)}{4IC_A} \tag{9}$$

$$\nu = \sqrt{\mu^2 - \frac{2mdC_{m_\alpha}}{\rho S I C_A^2}} \approx \sqrt{-\frac{2m^2 d C_{m_\alpha}}{\rho S I C_A^2}} \tag{10}$$

It should be noted that Eq. (9) differs slightly from the corresponding expression in Schoenenberger and Queen because the expression above does not utilize their approximation that $C_{L\alpha} = -C_A$ [2]. This approximation is derived from linearization of the drag and lift coefficient equations, the small angle approximation, and the assumption that $C_{N\alpha} \ll -C_A$. FF-CFD simulation results indicated that the latter of these assumptions was invalid for the case of the Genesis capsule and an alternative formulation was used for μ that does not rely on this assumption, presented by Schoenenberger et al. [4]. As reference, using the static aerodatabase generated by FF-CFD, at $\alpha = 0°$, the relative difference between $C_{L\alpha}$ and $-C_A$ was 15% and this discrepancy increases at higher angles of attack. As a contrast, the

assumption that $C_D \simeq C_A$ as required for Eq. (7) was found to be valid for the Genesis static data with the relative difference at $\alpha = 0°$ approaching 0 and at a relatively high α of 25°, the difference was 6%.

Finally, Eq. (7) assumes infinite velocity at $t = 0$, which necessitates a time shift for all presented simulations (which require finite initial velocities). This time shift is defined by Eq. (11), which again employs the approximation $C_A \simeq C_D$.

$$t_i = \frac{2m}{\rho V_i S C_A} \tag{11}$$

The static coefficients in Eq. (1) were assumed to be constant in the derivation by Schoenenberger and Queen [2]. However, FF-CFD static output showed some static aerodynamic coefficients to vary significantly as a function of angle of attack for the Genesis capsule. For example, $C_{L\alpha}$ at $0° = -1.226$ and $C_{L\alpha}$ at $20° = -1.032$, representing a 16% difference. Thus, in the data reduction and reconstruction, $C_{L\alpha}$ and C_A were calculated at each local angle of attack and not assumed constant, with the exception of C_A in the initial time shift for 3-DoF in Eq. (11). The calculated pitch damping coefficient was found to be insensitive to this change.

C. CADRA Curve Fitting of Analytical Solutions

The process to derive a pitch damping curve as a function of instantaneous angle of attack using the analytical solutions is shown below in Fig. 3. The approach for applying the analytical formulations to FF-CFD data to extract local pitch damping within a group of oscillation peaks and then fitting the CADRA function (Eq. (12)) to the collection of sectional fits is detailed further in Stern [1]. The pitch damping curve is found by solving for $C_{mq,1}$, $C_{mq,2}$, and $C_{mq,3}$ in Eq. (12) in the fitting. To enable use of the pitch damping curve in trajectory reconstruction, this work extends this process by introducing an additional step which converts the pitch damping curve from one that is a function of oscillation amplitude to a curve that is a function of instantaneous angle of attack.

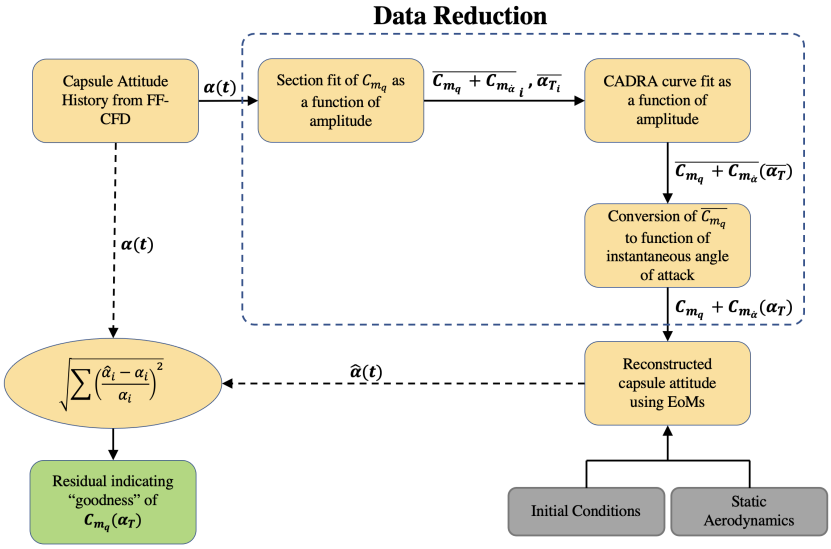

Fig. 3 Approach for deriving pitch damping curves through curve fitting of analytical solutions.

1. FF-CFD Sectional and Non-Linear Functional Fitting

Using the total angle of attack peaks, $\overline{\alpha_T}$, the amplitude growth is measured in stencils that include a user-specified three to five peaks per stencil. The local pitch damping coefficient, $(\overline{C_{m_q} + C_{m_{\dot{\alpha}}}})_i$, is calculated by considering the amplitude growth within a stencil and using the appropriate analytical expressions described in the previous sections. This local pitch damping coefficient is stored with the average amplitude of the stencil, $\overline{\alpha_{T_i}}$. This process is performed for all peaks in a set of trajectories that encompass a wide range of initial angles of attack. The local pitch damping coefficient with its corresponding average amplitude is plotted for each stencil and each initial angle of attack. The binned amplitude-pitch damping data are then curve-fit. In this work, only a single Mach number is being studied; therefore the Mach number can be treated as a constant in the fitting process and the CADRA function from Schoenenberger et al. [4]

reduces to Eq. (12). While the 3-DoF simulations are decelerating and therefore not at a constant Mach number, the application of this CADRA function to a single ballistic range shot typically uses the average Mach number across the shot for the purposes of fitting.

$$\overline{C_{m_q} + C_{m_{\dot{\alpha}}}} = max[(C_{mq,1} + C_{mq,2} \sin^2 \overline{\alpha_T}), (C_{mq,3})] \tag{12}$$

2. Conversion Between Amplitude and Instantaneous Space

Using the process described above, the pitch damping coefficient is only known as a function of the peak amplitude, $\overline{\alpha_T}$. Although this is useful for general intuition and identification of any existing limit cycle amplitude, explicit reconstruction of the trajectory requires knowledge of the pitch damping coefficient as a function of instantaneous angle of attack. Thus, the conversion strategy described by Bass Redd was employed [5]. This scheme assumes that the motion of the capsule can be described using Eq. (13) and Eq. (14), where motion is a function of instantaneous angle of attack and amplitude, respectively.

$$I\ddot{\alpha} + f(\alpha)\dot{\alpha} + k\alpha = 0 \tag{13}$$

$$I\ddot{\alpha} + f(\overline{\alpha})\dot{\alpha} + k\alpha = 0 \tag{14}$$

The only difference between these formulations is in the damping terms, $f(\alpha)$ and $f(\overline{\alpha})$, which include the pitch damping coefficient. Additional assumptions employed by this method are that the vehicle is symmetric in the pitch plane, the energy per cycle is equivalent between the two expressions, as shown by Eq. (15), and the damping term can be approximated as an even polynomial up to eight terms [5]. Through integration and matching like coefficients, a numerical equivalence of the polynomial coefficients is found, which is used to convert the curves. This transformation of having the pitch damping curve depend on the instantaneous angle of attack instead of the amplitude enables us to reconstruct the attitude of the vehicle using the equations of motion.

$$\int_0^T f(\alpha)\dot{\alpha}^2 dt = \int_0^T f(\overline{\alpha})\dot{\alpha}^2 dt \tag{15}$$

D. Attitude Reconstruction

The attitude history can be simulated once we know the initial state of the body (α_0 and $\dot{\alpha}_0$), the geometric and mass properties included in Eq. (1), and a curve that captures the pitch damping as a function of instantaneous angle of attack. This is performed by numerically integrating Eq. (1) as an initial value problem, in this instance using Python's scipy.integrate.solve_ivp function, which uses explicit Runge-Kutta 45 method [17].

E. Inverse Estimation of the Pitch Damping Curve

An alternative method to derive a pitch damping curve using an inverse estimation technique was also explored. This approach finds an optimal pitch damping curve as a function of instantaneous angle of attack through an optimization of the initial value problem seeking to minimize differences in the angle of attack peaks for reconstructed trajectories relative to the original data produced with FF-CFD. The normalized L_2 residual of the error between the peak magnitudes and peak times is minimized and achieved by changing the coefficients of the functional form that define the pitch damping curve (see Eq. (16)). This process is performed using the 1-DoF data with Python's scipy.optimize.minimize [18]. The gradient based method Powell was used for the analysis. Functional forms for the pitch damping curve investigated included CADRA [4], Aeroballistic Research Facility Data Analysis System (ARFDAS) [4], exponential, and cubic fit control points. Examples of each functional form for the pitch damping curve are presented in Fig. 4. Cubic fit control points involves specifying discrete α points with discrete pitch damping coefficient values and fitting a cubic interpolation between each respective point. The interpolation scheme utilized Python's scipy.interpolate.interp1d [19]. A schematic describing this methodology is in Fig. 5.

$$\text{Residual} = \sum_{min\alpha_0}^{max\alpha_0} \sqrt{\sum_{\alpha_{i=peak,0}}^{\alpha_{i=peak,n}} \left(\left(\frac{\hat{\alpha_i} - \alpha_i}{\alpha_i} \right)^2 + \left(\frac{\hat{t_i} - t_i}{t_i} \right)^2 \right)} \tag{16}$$

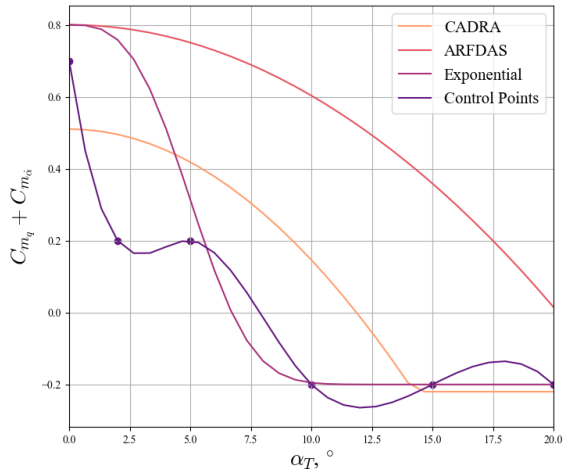

Fig. 4 Functional forms for inverse estimation of the pitch damping curve.

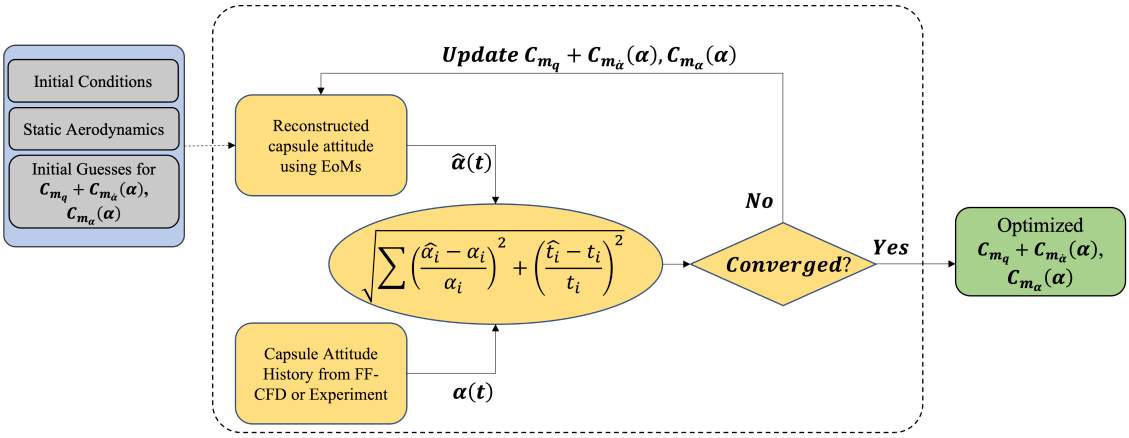

Fig. 5 Inverse approach for estimating pitch damping curve and pitch moment slope curves

In an effort to stress the inverse estimation and remove any bias regarding the assumed shape of the pitch damping curve, the control point estimation was run with a flat initial guess of $C_{m_q} + C_{m_\dot{\alpha}}(\alpha)$=0 for all α. The resultant shape of the pitch damping curve and the corresponding residuals were found to be insensitive to the initial guess, showing promise that this technique requires little to no knowledge of the pitch damping curve shape beforehand. However, the other functional forms were sensitive to the initial guess and performed poorly without tight constraints on the input coefficients or when atypical initial curves were input.

Finally, the limit cycle behavior of the trajectories was investigated using this inverse estimation technique. The trajectories simulated using the optimized pitch damping curve derived from this process were run until a limit cycle was achieved. The shorter timed initial amplitude runs are superimposed onto the long reconstructed trajectory and compared. Further, additional FF-CFD data were generated for an extended time span (1.5 seconds) at α_0 at 0.1°, 5°, and 10°for 1-DoF as a validation tool to probe the optimized inverse estimation curves, as well as compare the limit cycle noted in the reconstruction.

IV. Results

The reconstruction technique of applying CADRA curve fits to the analytical solutions described in Section III.C was applied to FF-CFD data. The the inverse estimation approach was applied to 1-DoF data using the Powell method and the cubic control points functional form.

A. Pitch Damping Curves Derived from CADRA Curve Fitting of Analytical Solutions

The oscillation history from 1-DoF FF-CFD data with initial angles of attack of 2°, 4°, and 10 ° are shown in Fig. 6a. Similarly, the oscillation history from 2-DoF FF-CFD data with the same initial angles of attack of 2°, 4°, and 10° are shown in Fig. 7a, and likewise history for 3-DoF in Fig. 8a. From this, it is shown that the contribution of C_{L_α} in the exponential growth terms of 2-DoF and 3-DoF (Eq. (6), Eq. (9), respectively) results in amplified oscillation growth for every initial angle of attack. Additionally, the deceleration present in the 3-DoF case further reduces damping in the system.

The pitch damping curve derived from section fits from the aforementioned 1-DoF trajectories using Eq. (12) is shown in Fig. 6b. The solid line represents the non-linear curve fit to the all binned section fit points. The dashed line (upper fit) is fit only to the subset of binned section fits that are greater than the original non-linear fit of all data and provides a means of assessing an upper bound of the pitch damping curve. Analogous results for 2-DoF and 3-DoF are shown in Fig. 7b and 8b. The neutral stability line shown in the pitch damping curves (Fig. 6b, Fig. 7b, and 8b) represents the pitch damping coefficient value for which the oscillation amplitude would stay constant. This is determined by setting the corresponding exponent in the analytical expressions (Equations 3, 6, 9) to zero and solving for $C_{m_q} + C_{m_{\dot{\alpha}}}$.

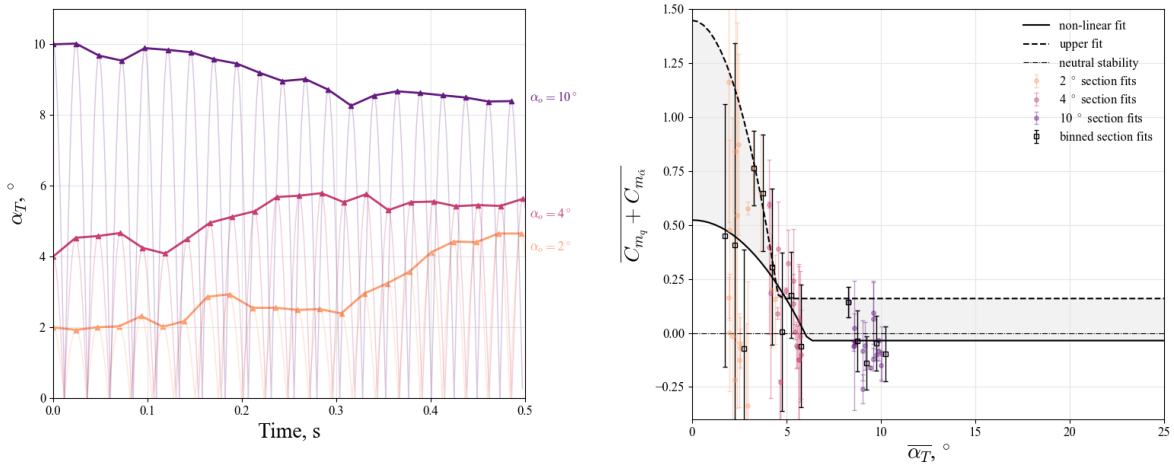

(a) (b)

Fig. 6 1-DoF FF-CFD generated trajectories (left) and associated non-linear pitch damping curve (right).

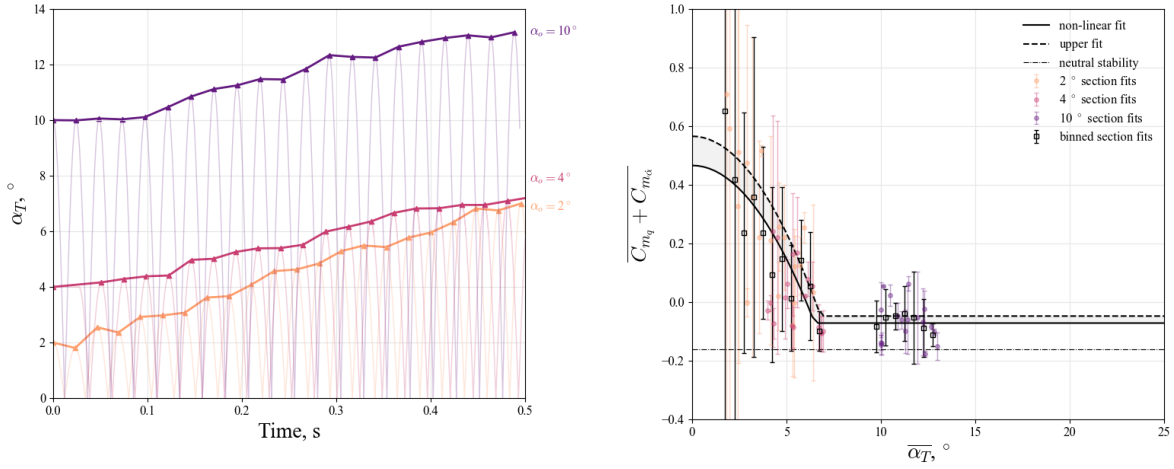

(a) (b)

Fig. 7 2-DoF FF-CFD generated trajectories (left) and associated non-linear pitch damping curve (right).

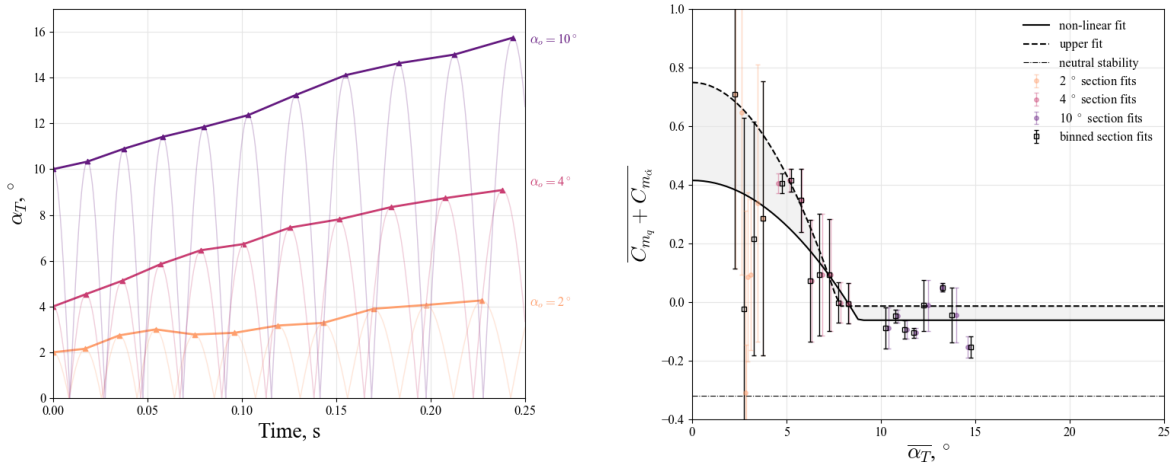

(a) (b)

Fig. 8 3-DoF FF-CFD generated trajectories (left) and associated non-linear pitch damping curve (right).

A comparison showing each respective pitch damping curve as a function of amplitude with the binned section fits is found in Fig. 9. This shows that the pitch damping curves derived from FF-CFD simulations covering a common set of initial amplitudes for 1-DoF, 2-DoF, and 3-DoF are statistically equivalent. This observation is consistent with the analytical formulation described in Section III.B and in Schoenenberger and Queen [2].

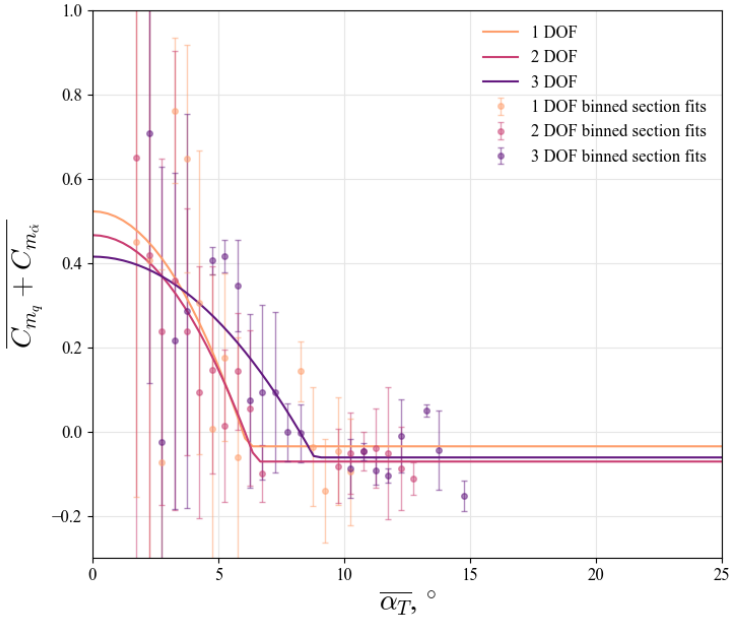

Fig. 9 Non-linear pitch damping curves generated from FF-CFD data.

Having established this equivalency, the remaining investigations focus on an expanded set of 1-DoF data with initial amplitudes (0.1°, 1°, 2°, 3°, 4°, 5°, 10°, and 20°), as shown in Fig. 10a. Figure 10b shows the pitch damping curve corresponding to this expanded set of FF-CFD data. Comparing this curve to that of Fig. 6b, it is clear that the addition of more simulation data at low angles of attack was necessary for appropriately capturing the true nature of the pitch damping curve, as the high pitch damping coefficient values in this regime result in an updated pitch damping curve that

indicates significant dynamic instability when the vehicle is at small angles of attack. This comparison is shown in Fig. 11a. The pitch damping curve beyond 5° remains relatively unchanged with the additional simulation data, again suggesting that best practice for this data reduction method should concentrate simulation data in the non-linear region of the pitch damping curve at low angles of attack.

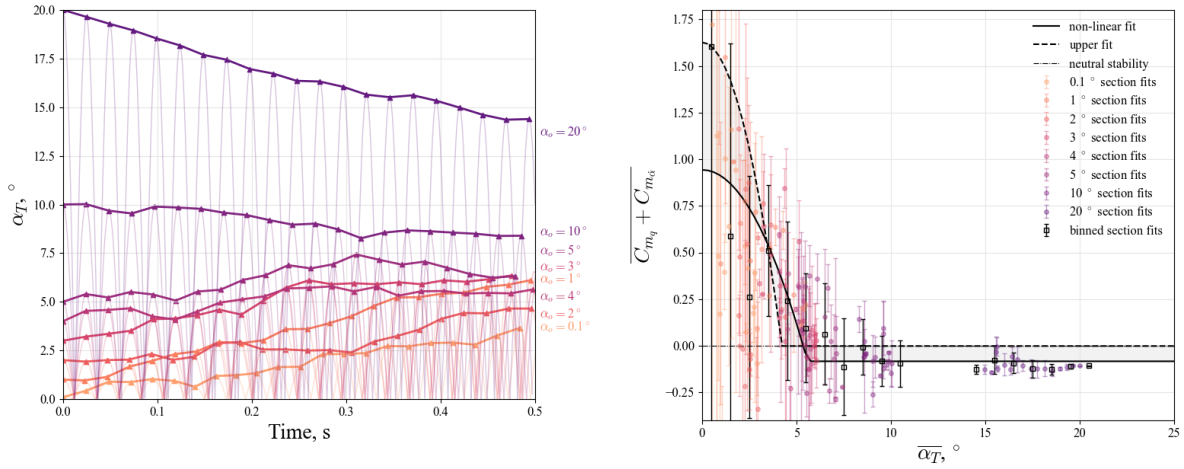

(a) (b)

Fig. 10 Expanded set of 1-DoF FF-CFD generated trajectories (left) and associated non-linear pitch damping curve (right).

B. Reconstruction of FF-CFD Trajectories

Application of the conversion technique described in Section III.C.2 yields the 1-DoF non-linear pitch damping curve as a function of instantaneous angle of attack found in Fig. 11b when using the expanded set of FF-CFD data shown in Fig. 10. The reconstruction of the α_T history using this curve was performed for the all 1-DoF initial amplitudes. The total residual for the set of trajectories is found by summing the normalized residual error of the peaks for each case. This is computed using Eq. (17) where there are n peaks in a given FF-CFD simulation. It may be noted that this residual does not take into account the time difference between the reconstructed peaks and the actual peaks as captured by Eq. (16) because this scheme requires $C_{m\alpha}$ in the frequency term stay constant, thus there is no means to compensate for the slight mismatch in frequency.

$$\text{Residual} = \sum_{min\,\alpha_0}^{max\,\alpha_0} \sqrt{\sum_{\alpha_{i=peak,0}}^{\alpha_{i=peak,n}} \left(\frac{\hat{\alpha}_i - \alpha_i}{\alpha_i}\right)^2} \tag{17}$$

C. Inverse Estimation of the Non-linear Pitch Damping Curve through Reconstruction

The optimized pitch damping and pitch moment slope curves found using the 1-DoF data-set with the cubic control points functional form and the Powell optimization method are found in Fig. 12a and Fig. 12b, respectively. These curves were generated using the FF-CFD 1-DoF data found in Fig. 10a with an initial amplitude range from 0.1° to 20°. The curve defining the initial guess for pitch damping coefficient (red line) is 0 for all α. The initial guess for the pitch moment slope (red line) is the static value at an angle of attack equal to 0° (-0.083 rad/s). This strategy aptly reproduced the common shape of the pitch damping curve as a function of angle of attack: a highly non-linear region at low amplitudes, a transition region, and a nearly constant region at high amplitudes.

Reconstructing the attitude history with these curves (Fig. 12a and Fig. 12b) shows good agreement with the FF-CFD data. The scheme's ability to capture the oscillation growth history irrespective of initial amplitude is shown in Fig. 13, where the initial reconstructed amplitude is 0.1° using the inverse estimation curves (gray curve). This 0.1° reconstruction is run for a prolonged time span (1.5 seconds) in an attempt to capture the full oscillation growth regime using the aforementioned pitch damping curve until a constant amplitude is noted. In this oscillation growth region, various FF-CFD data is overlaid near the closest reconstructed peak to the respective data's initial amplitude. As shown in Fig. 13, this is around 0.2 seconds for $\alpha_0 = 1°$, 0.3 seconds for $\alpha_0 = 2°$, 0.4 seconds for $\alpha_0 = 3°$, 0.6 seconds for

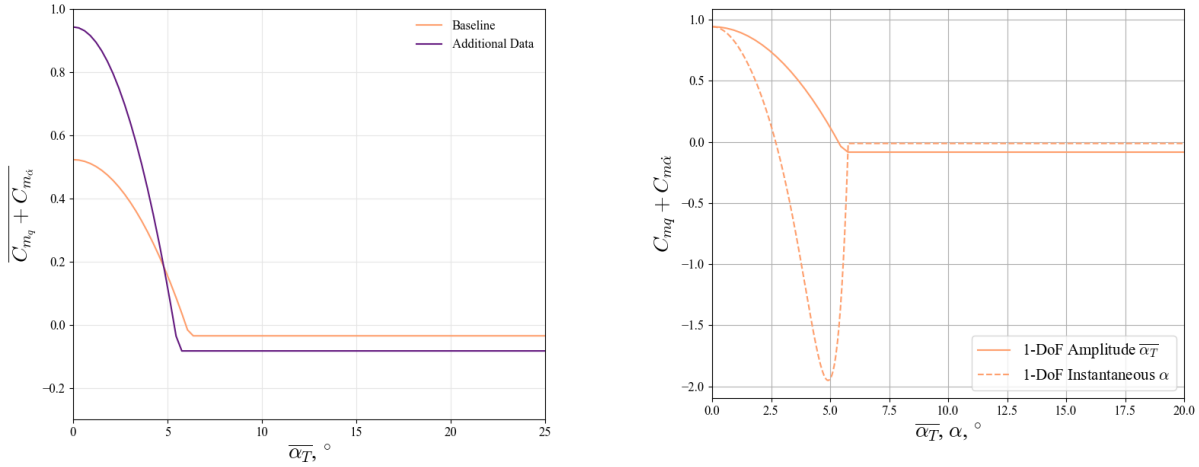

(a) (b)

Fig. 11 1-DoF FF-CFD baseline initial amplitudes (2°, 4°, 10°) versus expanded set of initial amplitudes (0.1°, 1°, 2°, 3°, 4°, 5°, 10°, 20°) (left) and CADRA converted pitch damping curve (left).

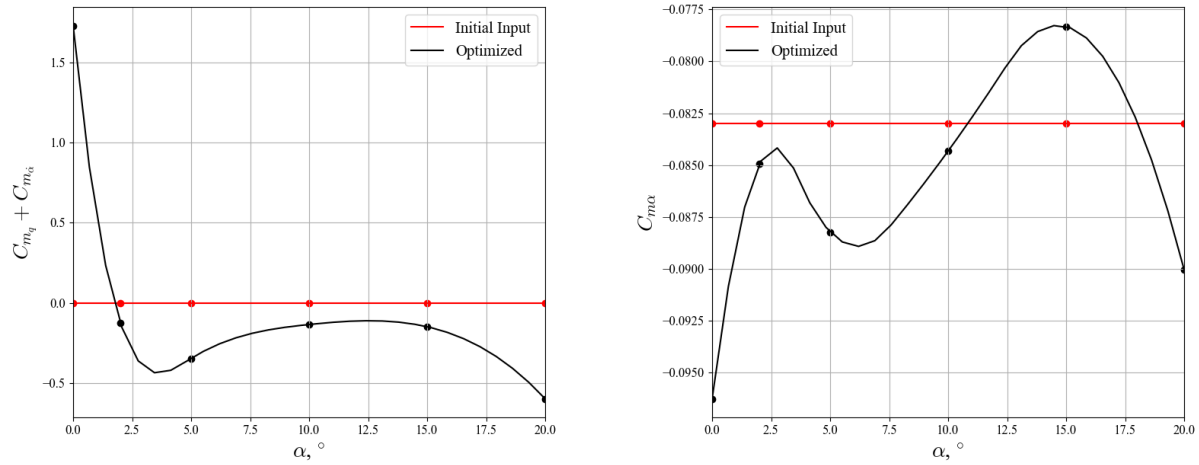

(a) (b)

Fig. 12 1-DoF FF-CFD pitch damping curve (left) and pitch moment slope curve (right) found through inverse estimation using the expanded set of initial amplitudes.

$\alpha_0 = 4°$, and 0.7 seconds for $\alpha_0 = 5°$. This shows that the full oscillation growth history reconstructed when starting at 0.1° and using the inverse estimation derived pitch damping curve curve closely captures the oscillation growth observed for each of the low initial amplitude FF-CFD data-sets.

D. Model Performance Comparison

The 1-DoF pitch damping curves for the two estimation methods, CADRA fits to the analytical solutions (orange) and the inverse estimation (purple), are shown in Fig. 14 with the respective reconstructed trajectories in Fig. 15. The pitch damping curves using CADRA fits to the analytical solutions as outlined in Section III.C were found to only result in moderate success during attitude reconstruction as shown in the orange curves in Fig. 15. The inverse estimation scheme was shown to simultaneously identify pitch damping and pitch moment slope curves which produce

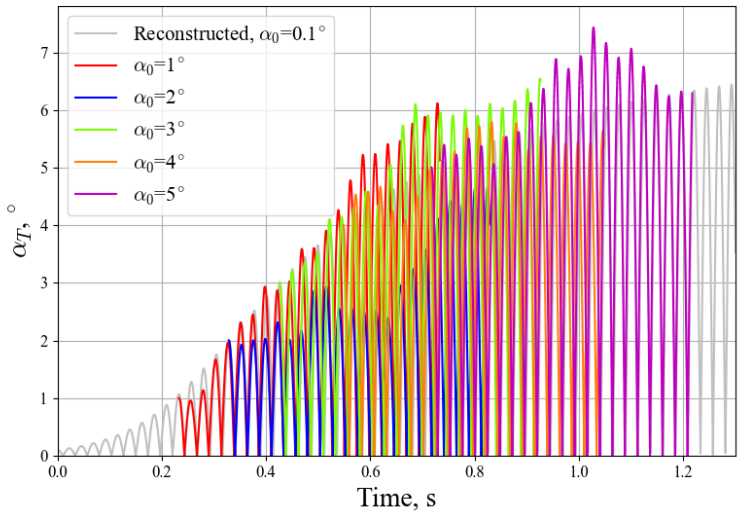

Fig. 13 Reconstructed trajectory using the inverse method for optimizing the pitch damping curve with low amplitude FF-CFD 1-DoF trajectories

reconstructed trajectories that are in excellent agreement with the FF-CFD data as shown in the purple curves in Fig. 15.

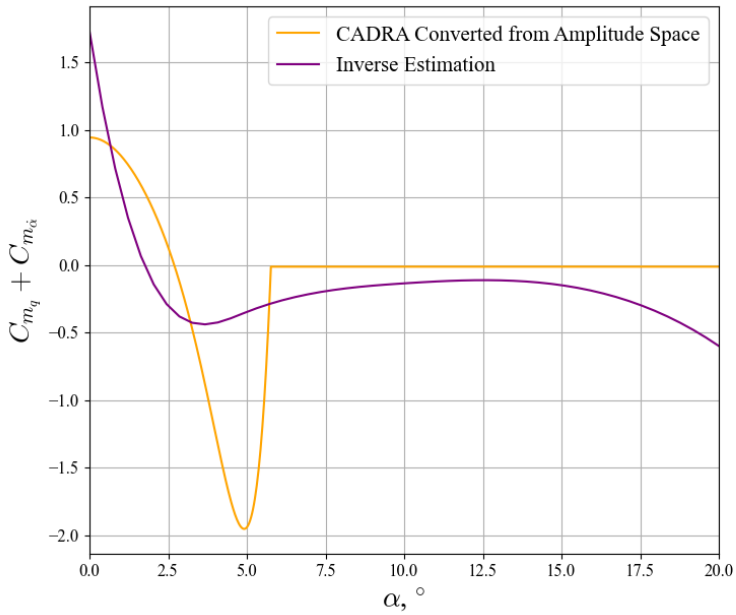

Fig. 14 1-DoF pitch damping curves as a function of instantaneous angle of attack derived from CADRA curve fitting of analytical solutions and inverse estimation

E. Validation Trajectories

Additional FF-CFD data which were run for a longer simulated time span (1.5 seconds) at α_0 at 0.1°, 5°, and 10° for 1-DoF are found in Fig. 16. These data were generated as a means of testing the ability of the derived pitch damping curves to predict the attitude history of data that was not used to train the original pitch damping curve formulation.

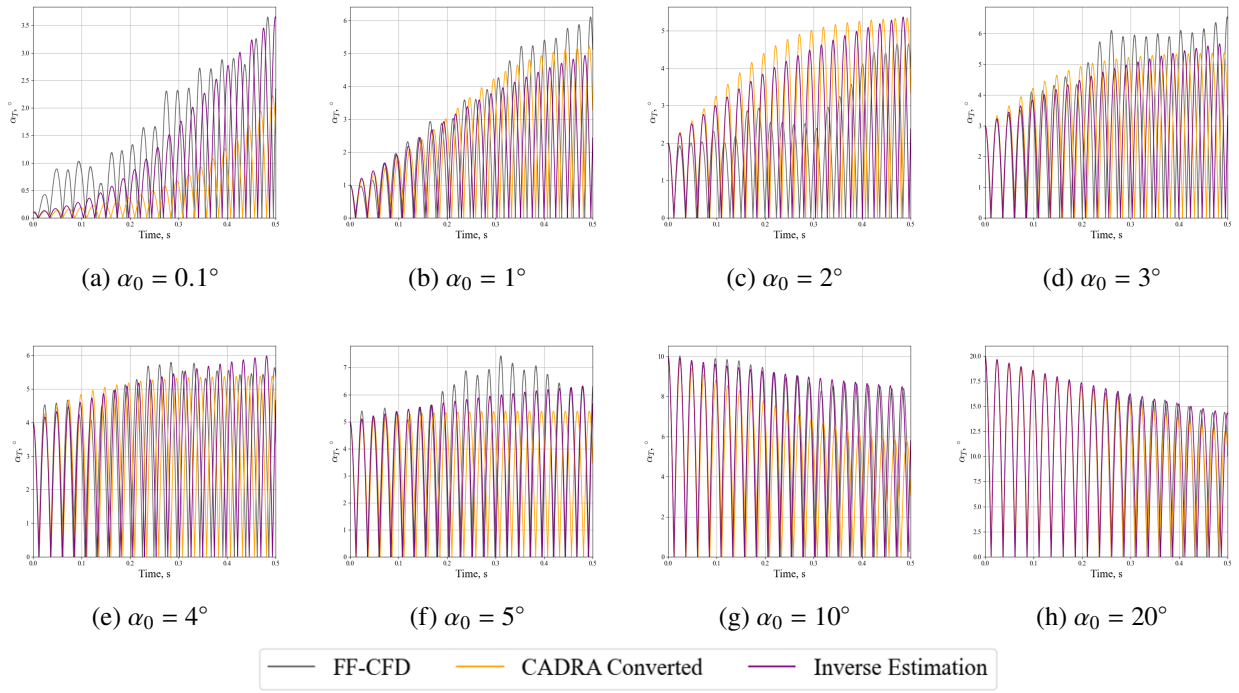

Fig. 15 Comparison between 1-DoF FF-CFD trajectories and reconstructions using both data reduction methodologies

Each of these longer trajectories approaches a similar limit-cycle amplitude with the increased time where the amplitude reaches a near equilibrium, in this case around 7°. The attitude history reconstructed with the optimized pitch damping curve derived from the inverse method using control points can be compared to this longer data-set as shown in Fig. 17a for α_0=0.1°. Similar agreement was found for each initial amplitude for the reconstructed and longer time data as seen in Fig. 17b and Fig. 17c. The purple reconstructed trajectories in Fig. 17 use the optimized pitch damping and pitch moment slope curves in Fig. 12a and Fig. 12b.

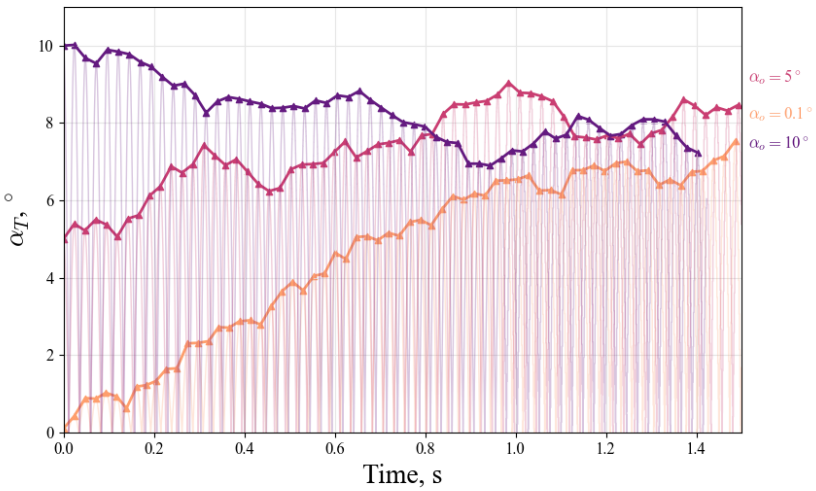

Fig. 16 1-DoF extended duration FF-CFD trajectories for validation

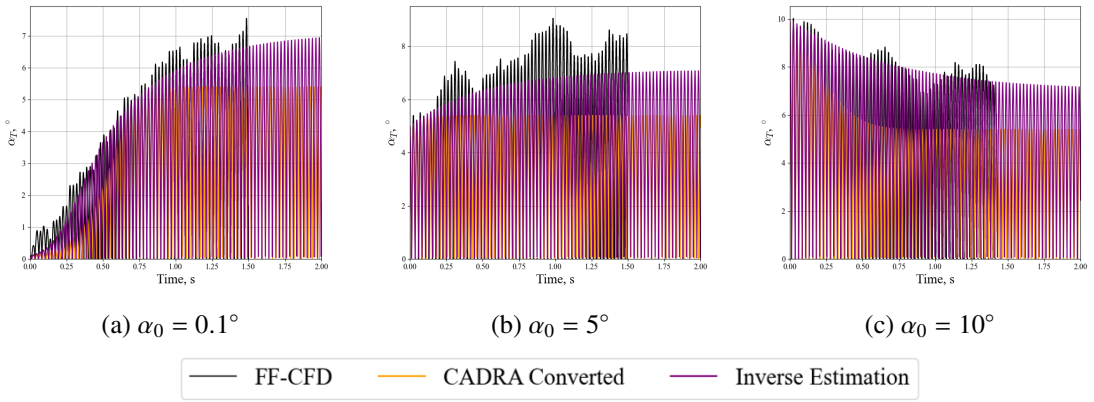

(a) $\alpha_0 = 0.1°$ (b) $\alpha_0 = 5°$ (c) $\alpha_0 = 10°$

Fig. 17 Comparison between long duration 1-DoF FF-CFD validation trajectories and reconstructions using both data reduction methodologies

V. Discussion

Comparing the pitch damping curves between degrees-of-freedom in Fig. 9 shows relative insensitivity to DoF when the data-sets have the same group of initial amplitudes. A noted difference, however, is the variability of the upper bound fit, particularly for 1-DoF. Understanding this behavior requires additional investigations to conclusively determine the cause. Further, including additional data from the the expanded data-set for 1-DoF results in a pitch damping curve with a greater pitch damping value at zero amplitude, as well as a steeper non-linear region. This highlights the curve's dependence on availability of low amplitude data as shown in Fig. 11a. The inflection point from non-linear to constant behavior in the curve, as well as the constant value at high amplitudes are similar between the two data-sets, indicating the addition of high amplitude data (20°) has less effect on the overall curve shape than the addition of low amplitude data.

It was found that the reconstruction using pitch damping CADRA curve converted from amplitude space was least accurate for 0.1° and 10° initial amplitudes (Fig. 15a and Fig. 15g, respectively), under-predicting the oscillation growth. Also shown is an over-prediction of oscillation growth for 2° . For blunt bodies it is typical for the damping to be low or negative at low angles of attack (recall that for 1-DoF, negative damping is associated with a $C_{m_q} + C_{m_{\dot{\alpha}}}$ value greater than zero). At higher angles of attack, the damping is high and the amplitude may stay constant or even shrink from peak to peak as shown for $\alpha_0 = 20°$ in Fig. 6a. The bi-modal damping behavior forces a piece-wise functional form for many pitch damping curves. This can be seen in the inflection point shown in Fig. 6b around 7° for the CADRA functional form. However, combining these two behaviors in either a piece-wise or continuous function results in some smoothing of the transition region, generally between 5° and 10°. It may be postulated that this smoothing, and the resultant steep well seen after converting to instantaneous angle of attack (Fig. 11b) had an effect on the reconstruction of 10°. Additional reasons for this under-damping for 10° as well as 0.1° may be a pitch damping value that is too low at zero amplitude, noted because the upper bound (Fig. 6b) pitch damping coefficient value is nearly 150% higher at zero amplitude. This high over-damping for the 10° case was not observed in the 20° case because the 20° FF-CFD data itself sees greater overall damping, and thus reconstructing with a curve that tends to over-damp results in a smaller residual. The over-damping for 2° (see Fig. 15c) was noted when reconstructing with both the CADRA converted (orange in Fig. 14) curve, as well as the inverse estimated curve (purple in Fig. 14), appears to be a reflection of the stochastic behavior inherent to the physics being simulated in the FF-CFD rather than the curve generation and reconstruction schemes.

It is apparent that the low amplitude cases are subject to more variability in the peak to peak behavior. This variability is due to the heightened sensitivity of the vehicle to dynamic back shell moments generated by stochastic wake features that can dominate the relatively weak stabilizing static moments inherent to blunt bodies at low angles of attack. Interactions with wake features are evident in most of the FF-CFD trajectories, though the 1-DoF cases appear to be the most sensitive to these interactions. An example of this behavior can be seen in the $\alpha_0 = 2°$ case (orange) in Fig. 6a between 0.1 and 0.15 seconds where the amplitude growth suddenly reverses for a few oscillation cycles. This translates to negative pitch damping coefficient section fits for the 2° case in Fig. 6b. The stochastic behavior associated with wake interactions makes the pitch damping coefficient more difficult to predict at these low amplitudes and adds uncertainty to the fitting process for the non-linear region of the pitch damping curve.

The steep negative well in the pitch damping curve as function of instantaneous angle of attack is noted, as can be seen in Fig. 11b between 3° and 6°, similar to the transition region referenced above. This steep non-linear behavior emerges in the conversion of the polynomial describing the behavior in instantaneous space. This steep well was found for all cases investigated and is a by-product of the polynomial coefficient matching presented by Redd [5]. The intensity of this well plays a large role in the reconstruction process, resulting in over-damping for higher amplitudes as shown in the 10° case in Fig. 15g. Determining if this is a physical blunt body characteristic or if this is purely a consequence of the modeling scheme is being investigated further with potential work planned for additional simulations near this transition region.

These inverse estimation generated pitch damping curves were optimized from an initial, constant input (red lines in Fig. 12a and Fig. 12b) highlighting this strategy's insensitivity to the initial guess. The residuals from the trajectories produced with the inverse method were approximately 30% less than those from the CADRA fits to the analytical solutions. This is especially noted at 0.1° and 10° in Fig. 15a and Fig. 15g, respectively, amplitudes with notable poor reconstruction performance for the CADRA converted curve. Further, the inverse estimation technique eliminates the complications of applying the analytical solutions to user-specified segments of the trajectory to generate section fits, requires no initial assumptions regarding the functional form of the pitch damping curve as a function of amplitude, and does not require intermediate conversion to instantaneous angle of attack. The use of cubic interpolated control points decouples the inverse method from reliance on any assumed functional form and is able to better capture the multi-modal behavior of the pitch damping curve. Given the steep slope of the pitch damping curve at very low angles of attack, there is an opportunity to include additional control points in that region to improve performance. Alternative functional forms were investigated with less success than the control points approach.

Comparing the 1-DoF derived pitch damping curves for the two estimation methods in Fig. 14 shows that the inverse estimation scheme results in a higher pitch damping value at low angles of attack and a shallower, wider region where the curve transitions from high non-linear to nearly linear. This curve shape results in low residuals and better reconstruction near this region as shown in Fig. 15f and Fig. 15g for 5° and 10°, respectively. These curves were both derived from applying their respective techniques to the eight 0.5 second long FF-CFD data-sets corresponding to a variety of initial amplitudes shown in Fig. 10. To validate their performance in predicting the behavior of FF-CFD data that the two models had not been previously exposed to, reconstruction was run out for up to 2.0 seconds of trajectory time and compared to previously withheld FF-CFD data that was run for 1.5 seconds. Comparing the reconstruction using each of these curves for the 1.5 second $\alpha_0 = 0.1°$ case in Fig. 17a shows the inverse estimation more closely matches the actual FF-CFD data. This trend holds for $\alpha_0 = 5°$ and $\alpha_0 = 10°$ in Fig. 17b and Fig. 17c, respectively. The normalized peak magnitude L_2 residuals (Eq. (17)) for these cases are found in Table 1.

Reconstruction Curve	$\alpha_0 = 0.1°$	$\alpha_0 = 5°$	$\alpha_0 = 10°$
CADRA Converted	2.88	3.62	4.21
Inverse Estimation	1.68	1.98	2.01

Table 1 Reconstructed trajectory peak magnitude residuals for 1.5s FF-CFD data-set.

VI. Conclusion and Future Work

The ability to derive a pitch damping curve and assess its performance when applied to new conditions is invaluable for mission design. These curves play a key role in assessing mission survivability in the entry, descent, and landing phase. Existing experimental techniques have a long history of application to blunt bodies, but have inherent limitations when attempting to reduce the data into an aerodynamic database that is required for flight simulations. FF-CFD allows for more complete data-sets from which to extract curve coefficients. The data reduction analysis presented by Schoenenberger and Queen was used to determine the pitch damping curve as a function of amplitude for FF-CFD data. This curve was then converted to be a pitch damping curve as a function of instantaneous angle using the strategy presented by Redd [5]. From this, the attitude was reconstructed by solving an initial value problem using the ordinary differential equation in Eq. (1), also derived by Schoenenberger and Queen [2]. Inverse estimation of the pitch damping coefficient as a function of instantaneous angle was demonstrated. This approach also enables simultaneous optimization of the pitch moment slope to control the oscillation frequency of the vehicle. The inverse estimation was found to produce favorable results with low residuals and curves that are insensitive to the initial guess. Additionally, the inverse estimation strategy eliminates subjective input in the data reduction, such as stencil length, bin width, and cut-off amplitude in the instantaneous conversion. Finally, cross validation when reconstructing from a low initial amplitude

and comparing other FF-CFD initial amplitude curves also showed the inverse scheme implemented was robust in application to trajectories that were not included as part of the optimization.

Given the observed success of the inverse estimation approach, future work will focus on refinement of this method including the addition of more control points in strategic locations, exploration of alternative optimization methods, and application of statistical estimation methods. Future investigations will also involve extension of the reconstruction strategy to additional Mach numbers and up to full six degrees-of-freedom (6-DoF) motion. The probabilistic nature of the dynamic behavior seen in the FF-CFD simulations will be explored more rigorously and considered within the estimation framework. Finally, options will be explored to more fully realize the the benefits of the rich data-sets produced when assessing vehicle dynamics computationally by infusing additional data products beyond the amplitude history into the data reduction approach for pitch damping.

Acknowledgments

The authors gratefully acknowledge the NASA Pathways program and the Entry Systems and Technology division at Ames Research Center for providing funding for this work. Further acknowledgement and gratitude is extended to Mark Schoenenberger and Leslie Yates for providing support.

References

[1] Stern, E. C., Brock, J. M., McKown, Q. E., and Kazemba, C. D., "A Method for Deriving Capsule Pitch-Damping Coefficients from Free-Flight CFD Data," *AIAA Journal*, *submitted*.

[2] Schoenenberger, M., and Queen, E. M., "Limit Cycle Analysis Applied to the Oscillations of Decelerating Blunt-Body Entry Vehicles," Tech. Rep. RTO-MP-AVT-152B, May 2008.

[3] Yates, L. A., and Chapman, G. T., "Aerodynamic Ballistic Range Analysis using Generalized Math Models," *AIAA Atmospheric Flight Mechanics Conference*, American Institute of Aeronautics and Astronautics, San Diego, CA, 1996.

[4] Schoenenberger, M., Yates, L., and Hathaway, W., "Dynamic Stability Testing of the Mars Science Laboratory Entry Capsule," *41st AIAA Thermophysics Conference*, American Institute of Aeronautics and Astronautics, San Antonio, Texas, United States of America, 2009.

[5] Redd, B., Olsen, D. M., and Barton, R. L., "Relationship Between the Aerodynamic Damping Derivatives Measured as a Function of Instantaneous Angular Displacement and the Aerodynamic Damping Derivatives Measured as a Function of Oscillation Amplitude," NASA Technical Note D-2855, Manned Spacecraft Center, Houston, Texas, June 1965.

[6] Candler, G. V., Subbareddy, P. K., and Brock, J. M., "Advances in Computational Fluid Dynamics Methods for Hypersonic Flows," *Journal of Spacecraft and Rockets*, Vol. 52, No. 1, 2015, pp. 17–28.

[7] Nompelis, I., Drayna, T. W., and Candler, G. V., "Development of a Hybrid Unstructured Implicit Solver for the Simulation of Reacting Flows Over Complex Geometries ," *34th AIAA Fluid Dynamics Conference*, The University of Minnesota, Portland, 2004, pp. 1–12.

[8] Nompelis, I., Drayna, T. W., and Candler, G. V., "A Parallel Unstructured Implicit Solver for Hypersonic Reacting Flow Simulation," *17th AIAA Computational Fluid Dynamics Conference*, The University of Minnesota, Toronto, 2005, pp. 1–17.

[9] Brock, J. M., Stern, E. C., and Wilder, M. C., "Computational Fluid Dynamics Simulations of Supersonic Inflatable Aerodynamic Decelerator Ballistic Range Tests," *Journal of Spacecraft and Rockets*, Vol. 56, No. 2, 2019, pp. 526–535.

[10] Hergert, J. D., Brock, J. M., Stern, E. C., Wilder, M. C., and Bogdanoff, D. W., "Free-Flight Trajectory Simulation of the ADEPT Sounding Rocket Test Using US3D," *AIAA AVIATION*, Denver, Colorado, 2017, pp. 1–21.

[11] Brock, J. M., "Progress on free-flight CFD simulation for blunt bodies in the supersonic regime," *International Planetary Probe Workshop*, Boulder, Colorado, 2018.

[12] Stern, E., Schwing, A., Brock, J. M., and Schoenenberger, M., "Dynamic CFD Simulations of the MEADS II Ballistic Range Test Model," *AIAA Atmospheric Flight Mechanics Conference*, American Institute of Aeronautics and Astronautics, Washington D.C., 2016, pp. 1–27.

[13] Fehlberg, E., "Classical Fifth-, Sixth, Seventh-, and Eighth-Order Runge-Kutta Formulas with Stepsize Control," Tech. rep., Huntsville, Alabama, October 1968.

[14] Cheatwood, F., Winchenbach, G., Hathaway, W., and Chapman, G., "Dynamic stability testing of the Genesis Sample Return Capsule," *38th Aerospace Sciences Meeting and Exhibit*, American Institute of Aeronautics and Astronautics, Reno, Nevada, 2000, pp. 1–11.

[15] Wright, M., "The Dragonfly Entry and Descent System," *16th International Planetary Probe Workshop (IPPW)*, Oxford, UK, 2019.

[16] Kreyszig, E., *Advanced Engineering Mathematics,*, Jon Wiley and Sons, Inc., New York, New York, 1988.

[17] "scipy.integrate.solve_ivp," `https://docs.scipy.org/doc/scipy/reference/generated/scipy.integrate.solve_ivp.html`, April 2021. Accessed: 13 May 2021.

[18] "scipy.optimize.minimize," `https://docs.scipy.org/doc/scipy/reference/generated/scipy.optimize.minimize.html`, 2021. Accessed: 13 May 2021.

[19] "scipy.interpolate.interp1d," `https://docs.scipy.org/doc/scipy/reference/generated/scipy.interpolate.interp1d.html`, 2021. Accessed: 08 November 2021.